

Comparative Thermodynamic Study on Exfoliated Graphite Nanoplatelets Systems Dispersed in Dimethylformamide and water at T= (293.15, 298.15 and 303.15) K

Florinela SIRBU¹, Ion ION², Alina Catrinel ION²

¹*Ilie Murgulescu* Institute of Physical Chemistry of Romanian Academy,
202 Splaiul Independentei str., 060021, Bucharest, Romania
E-mail: sflorinela@yahoo.com

²*Politehnica* University of Bucharest, Faculty of Applied Chemistry and
Material Science, 1-7 Polizu str., 011061, Bucharest, Romania
E-mail: i_ion@chim.upb.ro, ac_ion@yahoo.com

Abstract. The density, speed of sound and refractive index of diluted binary mixtures of exfoliated graphite nanoplatelets dispersed in water, and N,N-dimethylformamide, respectively, at different concentrations of solvate and at different temperatures have been measured. From the experimental data obtained, acoustic parameters such as the acoustic impedance, isentropic compressibility, specific refraction, space-filling factor, and relaxation strength were calculated for all compositions and temperatures. The results have been used to identify molecular interactions in the mixtures, including structural changes of exfoliated graphite nanoplatelets in polar solvents.

Key words: thermodynamic study; exfoliated graphite nanoplatelets (xGnP); aqueous binary mixtures; optical properties; acoustical properties.

1. Introduction

The thermodynamic study of binary systems containing exfoliated graphite nanoplatelets (xGnP) dispersed in water (H₂O), and N,N-dimethylformamide (DMF) respectively is important for understanding the physical-chemical behavior of liquid mixtures containing carbon-based nanomaterials. The acoustic and optical properties present considerable interest in extending the temperature range of thermodynamic data for systems containing exfoliated graphite nanoplatelets systems dispersed in dimethylformamide and water, respectively [1–4].

There is a variety of intermolecular interactions among graphene sheets in particular colloidal ones in solution [5–7]. The interactions between two colloid

particles in liquids are assumed to be the sum of two contributions: London–Van der Waals forces and *Electrical Double Layer* (EDL) forces. In addition, solvation forces, hydrophilic forces and sterical forces are also present in many colloidal systems and affect their colloidal behavior. The simulations revealed that the adsorption of the polar, organic solvent molecules such as NMP, particularly the single layer of solvent molecules confined on the graphene sheets form an energy barrier and prevent the approaching of the graphene sheets from a complete recombination. As the magnitude of the energy barrier is directly dependent on the affinity of the solvent to graphene, the scale of solvation forces is strongly affected by the chemistry of the solvents. The simulations suggest the following order for the ability to stabilize pristine graphene in suspensions: NMP>DMSO>DMF [8, 9].

Adsorption of water on carbon surfaces has been studied since 1968 by Kiselev *et al.* [10] Several simulations proved that water can be strongly adsorbed at low relative pressures by carbon adsorbents due to the potential overlap in small pores [11, 12].

Water is found to behave very differently while interacting with hydrophobic pristine graphene [13]. There are very few experimental studies of water interactions with the carbon-based nanomaterials flat surfaces, such as graphene or exfoliated graphite nanoplatelets [14, 15] even if these nanomaterials can be used as sorbents in environmental applications [16, 17].

When water is in contact with graphene, the hydrophobic graphene surface would disrupt the dynamic hydrogen bonds of water, resulting in significant translational and rotational entropy loss of water molecules [18]. In aqueous medium, attractive forces arise between hydrated graphene sheets [19]. Such forces are often referred as hydrophobic forces and explain why water is not a good solvent to disperse pristine graphene. Nevertheless, the electrostatic repulsion is among the most exploited, because it can be readily tuned by chemical modifications of the graphene surface [20]. In this way, the properties of graphene-based dispersions can be easily controlled by adjusting a variety of factors such as: pH, ionic strength and surface chemistry [21, 22].

As part of our project on the thermodynamic properties of liquid mixtures, [23-25] a comparison between the new measurements of density, speed of sound and refractive indices of the binary system $x\text{GnP}+\text{H}_2\text{O}$ with $x\text{GnP} + \text{DMF}$ [26] at various concentrations of $x\text{GnP}$ and different volumes of the solvents at $T = (293.15, 298.15, \text{ and } 303.15) \text{ K}$ are presented.

From the measured data, the optical and acoustical properties such as acoustic impedance, isentropic compressibility, specific refraction, space-filling factor and relaxation strength calculated through different equations.

This study reports new experimental data for density, speed of sound and refractive indices of the binary system $x\text{GnP} + \text{H}_2\text{O}$ at various concentrations of $x\text{GnP}$ and different volumes of the solvents at $T = (293.15, 298.15, \text{ and } 303.15) \text{ K}$; studies the influence of the solvents on the physical-chemical behavior of $x\text{GnP}$;

calculates acoustic and optical parameters such as acoustic impedance, adiabatic compressibility, specific refraction, space-filling factor and relaxation strength calculated through different equations from experimental density, speed of sound and refractive index results.

2. Experimental Section

2.1. Materials and Methods

xGnP containing a mass fraction more than 0.95 carbon was provided from XG Sciences, Lansing, MI, USA and was characterised in our laboratory. KBr, and N,N-dimethylformamide (DMF) have been supplied by Merck.

Exfoliated graphite nanoplatelets were used without any pretreatment because of their mass fraction purity higher than 0.99. The details of the chemicals used for samples preparation are given in the Table 1.

Table 1. Comparison of Experimental Densities (ρ), Speed of Sound (c), Refractive Indices (n_D) of Water with Literature Values at Temperatures of (293.15, 298.15 and 303.15) K

T/K	$\rho/\text{kg}\cdot\text{m}^{-3}$		$c/\text{m}\cdot\text{s}^{-1}$		n_D	
	Expt.	Lit.	Expt.	Lit.	Expt.	Lit.
water						
293.15	998.22	998.220 [27]	1484.26	1483.1 [27]	1.33300	1.33300 [27]
		998.206 [28]		1482.36 [29]		1.33297 [30]
298.15	997.04	997.043 [31]	1498.35	1497.40 [32]	1.33249	1.33240 [33]
		997.040 [34]		1496.20 [35]		1.33250 [36]
303.15	995.63	995.650 [28]	1510.61	1509.00 [36]	1.33187	1.33180 [37]
		995.600 [37]		1509.14 [38]		1.32500 [39]

Working solutions of different compositions xGnP + H₂O were prepared at 298.15 K using deionized and doubly distilled water. The aqueous mixtures were prepared by mixing known compositions of stock and water solutions in narrow-mouth, ground glasses. The binary solutions were kept in special airtight glass bottles to avoid evaporation. A volume of 100 cm³ stock solution of exfoliated graphite nanoplatelets (solute) of 0.001 g·cm⁻³ at 293.15 K was prepared by directly weighing the materials using an A&D GH-252 (Japan) analytical balance with an accuracy of ± 0.0001 g. The dispersion of solute + water was improved by addition of pure ethanol 0.1 cm³ to 15 cm³ stock solution. The initial composition of the solutions was prepared with a precision of ± 0.0002 g·cm⁻³. For each solute, six

samples with different specific compositions domain from (0 to 100) $\text{kg}\cdot\text{m}^{-3}$ in increments of $20 \text{ kg}\cdot\text{m}^{-3}$. For uniformity, all of the aqueous mixtures were dispersed using an ultrasonic bath. The uncertainty in the composition at samples preparation was estimated to be less than $\pm 0.0001 \text{ g}\cdot\text{cm}^{-3}$. Each sample was sonicated for 30 minutes at 303.15 K and measured immediately.

The density and speed of sound of stock binary mixtures were measured with an Anton Paar DSA 5000 digital (Austria) analyser with a precision of $\pm 0.000001 \text{ g}\cdot\text{cm}^{-3}$. During the measurements of the density the temperature was controlled at a precision of $\pm 0.001 \text{ K}$, and several Peltier units have been used. The internal calibration of the instrument was confirmed by measuring the density and speed of sound in atmospheric air and doubly distilled deionised water, according to the recommendations of the manufacturer. Similar to the results described in the literature, the density of water was measured as $0.99704 \text{ g}\cdot\text{cm}^{-3}$ at 298.15 K [31, 34]. The values of ρ and c were reproducible within $\pm 0.000005 \text{ g}\cdot\text{cm}^{-3}$ and $\pm 0.05 \text{ m}\cdot\text{s}^{-1}$, respectively. The refractive indices were measured using an Anton Paar GmbH Abbe automatic refractometer with an accuracy of ± 0.000001 , and the temperature of the samples was controlled within $\pm 0.01 \text{ K}$. The refractometer was calibrated by measuring the refractive index of doubly distilled and deionized water. The refractive index of water was measured as 1.33249 at 298.15 K , which is similar to the value mentioned in the literature of 1.33250 [33, 34]. The samples were introduced into the cell (prism assembly) using a syringe. At least three independent measurements were done for each sample at each temperature to assure the effectiveness of the measurement. All the measurements were repeated at least three times and were repeatable within the level of precision quoted for the apparatus. Uncertainties associated with the experimentally data such as density, ultrasonic speed and refractive index were estimated based on the uncertainty of the measurement [40] and presented together with the experimental results in the tables.

2.2. Theory and Calculation

The following thermodynamic acoustical and optical parameters have been estimated using the standard relations employed in previous studies [41–46]. The acoustic impedance (Z) has been calculated using the following relation [41]:

$$Z = \rho c \quad (1)$$

where ρ is the density ($\text{kg}\cdot\text{m}^{-3}$), and c is the speed of sound ($\text{m}\cdot\text{s}^{-1}$) in the mixture.

The isentropic compressibility coefficient k_s for the pure solvent and liquid mixtures have been estimated from the density ρ and the speed of sound c using the Laplace equation [42].

$$k_S = \frac{1}{K} = \frac{1}{\rho c^2} \quad (2)$$

where, K is the bulk modulus of the solution.

According to the method of Gerecze [43] and Lorentz-Lorenz [44], the space-filling factor (S) has been computed from refractive index (sodium D line) data using the following relation [45]:

$$S = \frac{B}{V} = \frac{n_D^2 - 1}{n_D^2 + 2} \quad (3)$$

where, B is the effective volume occupied by molecules per mole, V is the molecular volume and n_D is the refractive index of the aqueous solution.

The specific refraction (r_D) has been estimated from the density (ρ) and space-filling factor (S) using the Lorentz and Lorenz equation, which is based on the electromagnetic theory of light, where as the other equations are of empirical origin [46]:

$$r_D = \frac{n_D^2 - 1}{n_D^2 + 2} \frac{1}{\rho} \quad (4)$$

The relaxation strength (r) has been calculated using the following equation [45]:

$$r = 1 - \frac{c^2}{c_{ct}^2} \quad (5)$$

where, c is the speed of sound in the experimental solution, and c_{ct} is a constant with a value of $1600 \text{ m}\cdot\text{s}^{-1}$ [46].

The specific concentration dependence on density and on ultrasound speed obtained in the two systems was correlated by a polynomial type equation:

$$F(Y) = \sum_{i=1}^n A_i C^{i-1} \quad (6)$$

where, Y represents the properties measured in general (ρ , c) and C represents the specific concentration.

Correlations of ρ , c , k_S and r as a function of concentration (Eq. 7) along with the absolute average percentage deviation (AAD) were analyzed. The absolute average percentage deviation (AAD %) was determined using the following relationship:

$$AAD(Y) = \frac{100}{N} \sum_i^n \left| \frac{Y_{\text{Expt.}} - Y_{\text{Calc.}}}{Y_{\text{Expt.}}} \right| \quad (7)$$

where N is the number of experimental data points. The subscripts “Expt.” and “Calc.” represent the values of the experimental and calculated property, respectively.

3. Results and Discussion

In order to characterize the interactions between solvent molecules and graphene we experimentally determined the thermodynamic parameters: density, ultrasound speed and refractive indices for xGnP dissolved in two solvents: DMF and H₂O, observing that DMF was a more effective solvent in comparison with H₂O.

The carbon based nanoparticles (xGnP) dispersed in DMF solvent were characterized previously [26] and discussed there. The experimental data of densities, ultrasound speed and refractive indices as a function of the specific concentration of xGnP in DMF and in water are presented in Table 2.

Table 2. Experimental Values of the Density ρ , Ultrasound Speed c and Refractive Index n_D at Various Temperatures T and Specific Concentrations C of xGnP, for the Binary xGnP + H₂O^a Mixture

T/K	$\rho/\text{kg}\cdot\text{m}^{-3}$	$c/\text{m}\cdot\text{s}^{-1}$	n_D	$\rho/\text{kg}\cdot\text{m}^{-3}$	$c/\text{m}\cdot\text{s}^{-1}$	n_D
	$C/\text{kg}\cdot\text{m}^{-3} = 0$			$C/\text{kg}\cdot\text{m}^{-3} = 20$		
293.15	998.22	1484.26	1.33300	997.50	1486.97	1.33327
298.15	997.04	1498.35	1.33249	996.35	1500.73	1.3328
303.15	995.63	1510.61	1.33187	994.95	1512.76	1.33223
	$C/\text{kg}\cdot\text{m}^{-3} = 40$			$C/\text{kg}\cdot\text{m}^{-3} = 60$		
293.15	996.81	1489.82	1.33343	996.18	1492.69	1.333597
298.15	995.66	1503.31	1.33294	995.04	1505.86	1.33305
303.15	994.27	1515.07	1.33238	993.64	1517.35	1.33244
	$C/\text{kg}\cdot\text{m}^{-3} = 80$			$C/\text{kg}\cdot\text{m}^{-3} = 100$		
293.15	995.44	1494.97	1.33366	995.05	1497.56	1.33399
298.15	994.31	1507.87	1.33317	993.90	1510.25	1.33350
303.15	992.88	1519.43	1.33260	992.50	1521.3	1.33292

^a $C/\text{kg}\cdot\text{m}^{-3}$ is the specific concentration of xGnP in the H₂O solvent. Standard uncertainties u are $u(T) = 0.001$ K for ρ and c ; $u(T) = 0.01$ K for n_D and the combined expanded uncertainties U_c are $U_c(\rho) = 0.01$ $\text{kg}\cdot\text{m}^{-3}$, $U_c(c) = 0.05$ $\text{m}\cdot\text{s}^{-1}$; (level of confidence = 0.95, $k = 2$) and $U_c(n_D) = 0.00001$.

Based on the values of the measured properties, the derived thermophysical parameters as a function of the specific concentration fraction at three different

temperatures between (293.15 and 303.15) K were calculated and presented in Table 3.

Table 3. Calculated Values of the Acoustic Impedance Z , Adiabatic Compressibility k_S , Space Filling Factor S , Specific Refraction r_D , and Relaxation Strength r at Various Temperatures T , Specific Concentration C of (xGnP), for the System xGnP+ H₂O

T/K	$\frac{Z}{10^5 \cdot \text{kg} \cdot \text{m}^{-2} \cdot \text{s}^{-1}}$	$\frac{k_S}{10^{-10} \cdot \text{m}^2 \cdot \text{N}^{-1}}$	S	$\frac{r_D}{10^{-3} \cdot \text{m}^3 \cdot \text{kg}^{-1}}$	r
$C/\text{kg} \cdot \text{m}^{-3} = 0$					
293.15	14.81617	4.54731	0.20569	0.20606	0.13944
298.15	14.93907	4.46748	0.20541	0.20602	0.12303
303.15	15.04015	4.40145	0.20506	0.20596	0.10862
$C/\text{kg} \cdot \text{m}^{-3} = 20$					
293.15	14.83247	4.53403	0.20584	0.20636	0.13630
298.15	14.95246	4.45641	0.20558	0.20633	0.12024
303.15	15.05124	4.39195	0.20527	0.20631	0.10608
$C/\text{kg} \cdot \text{m}^{-3} = 40$					
293.15	14.85069	4.51980	0.20594	0.20666	0.13298
298.15	14.96790	4.44417	0.20566	0.20656	0.11721
303.15	15.06389	4.38158	0.20535	0.20653	0.10334
$C/\text{kg} \cdot \text{m}^{-3} = 60$					
293.15	14.86989	4.50529	0.20603	0.20682	0.12964
298.15	14.98385	4.43192	0.20572	0.20675	0.11421
303.15	15.07703	4.37118	0.20538	0.20670	0.10064
$C/\text{kg} \cdot \text{m}^{-3} = 80$					
293.15	14.88146	4.49492	0.20607	0.20701	0.12697
298.15	14.99290	4.42334	0.20579	0.20697	0.11184
303.15	15.08616	4.36255	0.20547	0.20695	0.09817
$C/\text{kg} \cdot \text{m}^{-3} = 100$					
293.15	14.90147	4.48112	0.20625	0.20727	0.12395
298.15	15.01039	4.41122	0.20597	0.20724	0.10904
303.15	15.09896	4.35349	0.20565	0.20721	0.09596

The density, ultrasound speed and refractive index values as a function of specific concentration of exfoliated graphite nanoplatelets (xGnP) are shown in Figs. 1, 2 and 3, respectively, by comparison between both binary xGnP + DMF [26] and xGnP + H₂O systems, along of polynomial correlated values (ρ , c).

Fitting parameters A_i and absolute average percentage deviation results are reported in Table 4 for binary AC in DMF mixtures at all temperatures studied.

Table 4. Fitting Parameters A_i , Correlation Coefficient (R^2) Obtained for Density ρ , Ultrasonic Speed c , Isentropic Compressibility k_S and Relaxation Strength r Along with the Absolute Average Percentage Deviation (AAD %) for Binary xGnP + H₂O Mixture.^a

T/K	C/kg·m ⁻³	A ₁ /kg·m ⁻³	A ₂ /kg ⁰ ·m ⁰	A ₃ /kg ⁻¹ ·m ³	A ₄	R ²	AAD %
ρ/kg·m⁻³							
293.15	0-100	998.24	- 0.038815	0.000065	-	0.99771	0.004
298.15	0-100	997.06	- 0.037489	0.000055	-	0.99809	0.004
303.15	0-100	995.66	- 0.037510	0.000054	-	0.99711	0.005
T/K	C/kg·m ⁻³	A ₁ /kg ⁰ ·m ⁻¹ ·s	A ₂ /kg·m ⁻⁴ ·s	A ₃ /kg ² ·m ⁻⁷ ·s	A ₄	R ²	AAD %
c/m·s⁻¹							
293.15	0-100	1484.20	0.1462429	-0.0001286	-	0.99953	0.005
298.15	0-100	1498.30	0.1294214	-0.0001018	-	0.99939	0.004
303.15	0-100	1510.53	0.1185571	-0.0001036	-	0.99960	0.004
T/K	C/kg·m ⁻³	A ₁	A ₂	A ₃	A ₄ ·10 ⁻⁹	R ²	AAD %
n_D							
293.15	0-100	1.332991	0.000019086	- 0.000000266	2	0.99306	0.006
298.15	0-100	1.332485	0.000018383	- 0.000000254	2	0.99838	0.007
303.15	0-100	1.331875	0.000025157	- 0.000000425	3	0.99952	0.005
T/K	C/kg·m ⁻³	A ₁ /10 ⁻¹⁰ ·kg ⁰ ·m ² ·N ⁻¹	A ₂ /10 ⁻¹⁰ ·kg ⁻¹ ·m ⁵ ·N ⁻¹	A ₃ /10 ⁻¹⁰ ·kg ² ·m ⁸ ·N ⁻¹	A ₄	R ²	AAD %
k_S/10⁻¹⁰·m²·N⁻¹							
293.15	0-100	4.5475657	- 0.0007185	0.0000006	-	0.99889	0.014
298.15	0-100	4.4677032	- 0.0006030	0.0000004	-	0.99854	0.013
303.15	0-100	4.4017500	- 0.0005243	0.0000004	-	0.99954	0.007
T/K	C/kg·m ⁻³	A ₁ /kg ⁰ ·m ⁰	A ₂ /kg ⁻¹ ·m ³	A ₃ /kg ⁻² ·m ⁶	A ₄	R ²	AAD %
r							
293.15	0-100	0.1395071	- 0.0001697	0.0000001	-	0.99954	0.152
298.15	0-100	0.1230932	- 0.0001518	0.0000001	-	0.99940	0.109
303.15	0-100	0.1087068	- 0.0001404	0.0000001	-	0.99959	0.111

^aA_i and R² were obtained from Eq. 7; AAD %: $AAD(Y) = \frac{100}{N} \sum_i^n \left| \frac{Y_{Expt.} - Y_{Calc.}}{Y_{Expt.}} \right|$, where N = 6 number

of experimental data at each temperature.

Figure 1 presents the density as a function of the solute concentration of the binary mixtures xGnP + DMF [26] and xGnP + H₂O at various temperatures.

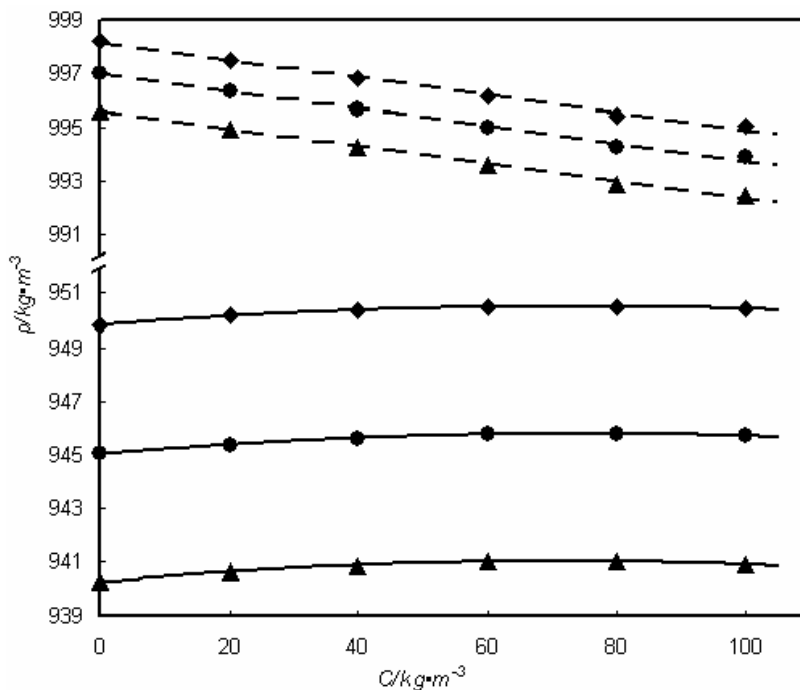


Fig. 1. Comparative representation of the density of binary xGnP + H₂O and xGnP + DMF [26] systems versus concentration of solute at various temperatures,
 T/K: ◆, 293.15; ◐, 298.15; ▲, 303.15; ---, for H₂O; —, for DMF; polynomial correlated values.

Good dispersion of graphene is influenced by the solubility parameters and surface tensions of the solvents, being found that an efficient solvent has a surface tension equivalent to that of graphene [47]. Good solvents for graphene provide stable colloidal dispersions for nanosized graphene.

Solvent molecules alone cannot exfoliate graphene, ultrasonic treatment being necessary. When the graphene sheets achieve certain separation by the ultrasonic treatment, the solvent molecules can insert between the graphite layers providing a colloidal stability.

The density of the binary system xGnP + DMF decreases by increasing the temperature and increases by increasing the concentration of the solute. Slight differences were observed between the two systems, indicating that DMF changes the structure of xGnP more strongly than water. These differences may be due to the number and position of oxygen-containing groups at the edges of xGnP, which improves the dispersion of the nanomaterial in DMF. These results support the

conclusion that a π - π interaction [48] occurs between carbon-based nanomaterials and DMF, which increases the density by increasing the mole fraction of the mixture.

The density profiles for the organic solvents suggest stronger interaction between the graphene surface and the DMF molecules, no clear isolated solvent layer being observed near the graphene surface in H_2O . There exists an enrichment of solvent layer near the graphene surface in both solvents, but the average interactions energies between the surrounding solvent molecules and the graphene is different. The dependence of the velocity of ultrasound on the concentration of $xGnP + DMF/H_2O$ is presented in Fig. 2.

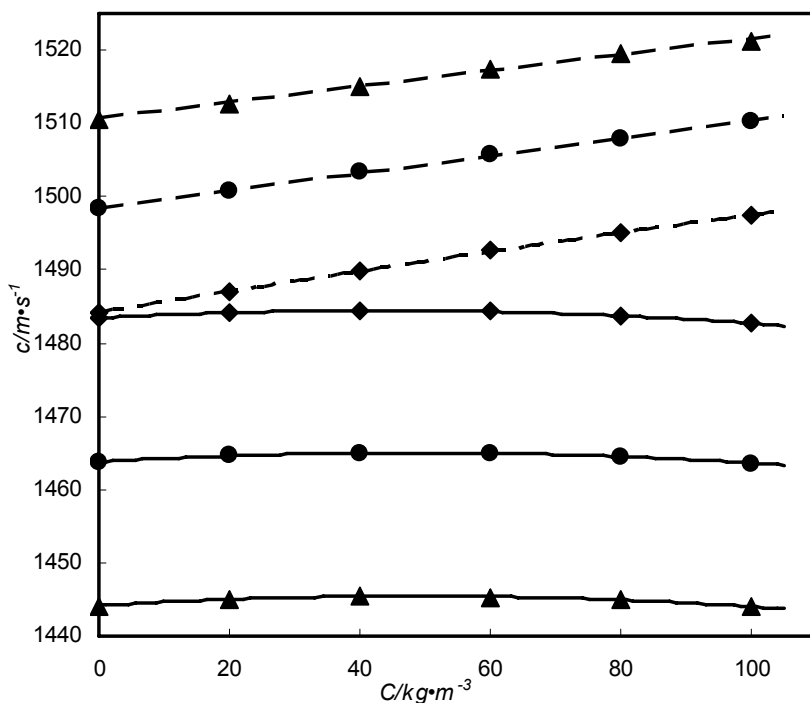


Fig. 2. Comparative representation of the ultrasound speed of binary $xGnP + H_2O$ and $xGnP + DMF$ [26] systems versus concentration of solute at various temperatures, T/K : \blacklozenge , 293.15; \bullet , 298.15; \blacktriangle , 303.15; $---$, for H_2O ; $—$, for DMF; polynomial correlated values.

As shown in Fig. 2, the ultrasound speed slightly increased with an increase in the concentration of the solute, indicating the presence of solute-solvent interactions *via* hydrogen bonding, which can produce displacements of electrons and nuclei in this range of concentrations. It slightly decreases with the temperature, much more for the $xGnP + DMF$ system. As the temperature

increased, the thermal energy leads to the breaking of the bonds and it weakens the molecular forces which decreases the ultrasound speed.

After the equilibrium, it can be presumed that DMF molecules can spread over the graphene surfaces, forming a complete solvent layer, this demonstrating that the graphene surface is solvophilic for the organic solvents [49]. The interaction between the organic molecules and graphene is larger than the inherent intermolecular interactions between the solvent molecules. Meanwhile, the water solvent just shows a hydrophobic dispersion interaction with the graphene surface. It is interesting to note that the attraction forces are approximately the same in different solvent media, which is determined by the attractive interaction between graphene sheets, being clear that the initial exfoliation is less dependent upon the solvent medium and the ultrasound speed will not have a significant variation in different solvents. The dependence of the refractive indices on the concentration of the solute (active carbon and exfoliated graphite nanoplatelets) in DMF is presented in Fig. 3.

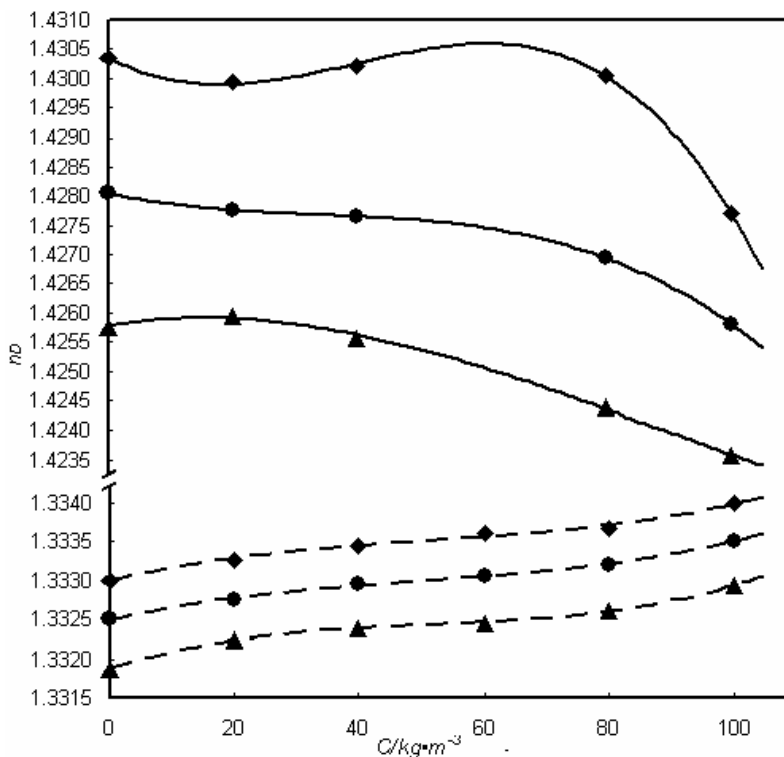


Fig. 3. Comparative representation of the refractive index of binary xGnP + H₂O and xGnP + DMF systems versus concentration of solute at various temperatures,

T/K: ♦, 293.15; •, 298.15; ▲, 303.15; --, for H₂O; —, for DMF [26];
polynomial correlated values.

Regardless of the temperature, at a concentration of 0.08 g mL^{-1} , the value of the refractive index and the space-filling factor increased, suggesting that dispersion improves for a specific concentration of xGnP in DMF. In comparison, variations in the refractive indices were not detected in water at the same concentration.

The repulsive forces which appear originate from the solvent-induced interactions. These forces are favourable to promote exfoliation and prevent aggregation. At very large separation, the force approaches to zero, indicating a complete detachment, this suggesting that in the exfoliation process the interfacial resistance at the beginning of graphene exfoliation is from the attractive interaction between graphene layers and then the solvent-induced force dominantly influence the subsequent exfoliation process. The repulsive force in organic solvent is higher than in the water solvent, this consisting with the enhanced interaction strength between the organic solvent and the graphene surface. The repulsive forces play a role in the attractive interaction between graphene sheets. In the water solvents, the solvent-induced forces present a weak interaction, blocking the parallel exfoliation.

The total resisting force is originating from the attractive interaction between the graphene sheets. In organic solvents, the solvent-induced force can give rise to the repulsive force to aid the exfoliation process, because of the stable confined solvent layer accommodated in the gap between the shifted graphene sheet and the fixed graphite.

In the water solvent, the confined solvent layer is not well accommodated because of the weak surface affinity. The water-induced force from the outer solvent molecules is the main controlling factor of the resisting action of the sheet moving [47].

The dependence of the isentropic compressibility on the concentration of the solute is presented in Fig. 4.

As shown in Fig. 4, the isentropic compressibility of the two binary systems increases with an increase in temperature. In the xGnP + DMF system, the isentropic compressibility decreases by increasing the concentration up to $0.06 \text{ g}\cdot\text{mL}^{-1}$, then increased for $C = 0.1 \text{ g}\cdot\text{mL}^{-1}$. The observed increase and decrease in the isentropic compressibility as a function of the concentration in the xGnP + DMF binary mixture were indicative of interactions between component molecules.

Isentropic compressibility is varies in a reversed dependence to the square of the ultrasound of speed, and its deviation can be attributed to the loss of di-polar association between the solvent molecules and differences in the size and shape of xGnP molecules, which reduces the velocity and increases the compressibility.

Dipole-dipole interactions or hydrogen-bonded complex formation between unlike molecules increased the velocity of ultrasound and decreased the compressibility. In the xGnP + H₂O system, the first mode of adsorption is characterized by water interactions within the graphene layers that are stacked to form graphitic microstructures of carbogenic materials [50].

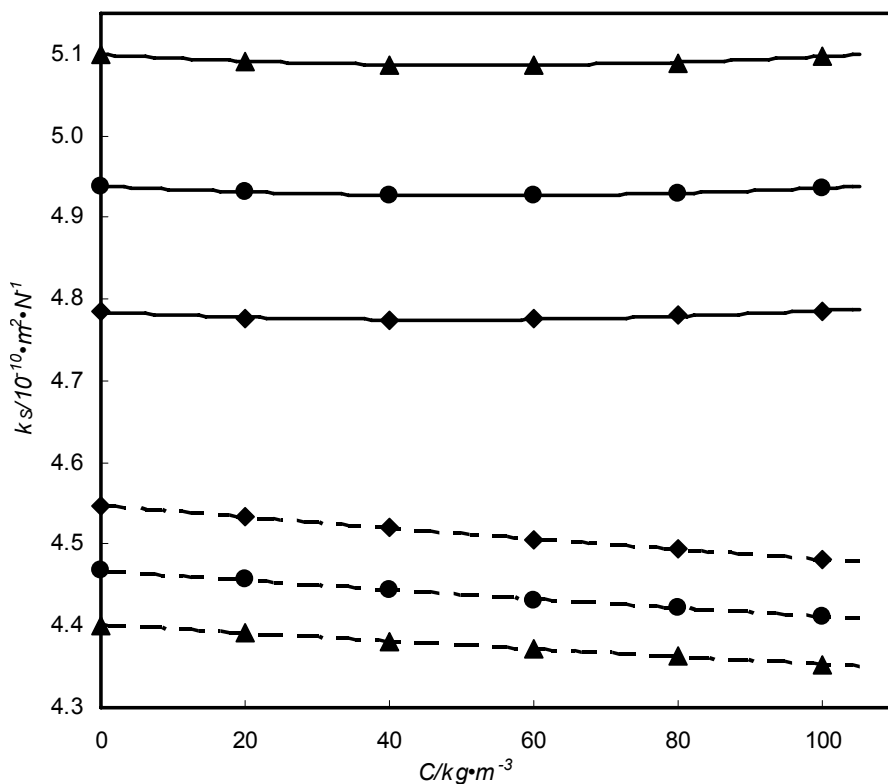


Fig. 4. Comparative representation of the isentropic compressibility of binary xGnP + H₂O and xGnP + DMF systems versus concentration of solute at various temperatures, T/K: \diamond , 293.15; 298.15; \blacktriangle , 303.15; --, for H₂O; —, for DMF [26]; polynomial correlated values.

The graphene layers offer a small attraction for water molecules, the micropores will adsorb water, the adsorption being followed by cooperative interactions of the adsorbed water with the other water molecules until filling of the graphitic microstructures occurs. The second mode of adsorption occurs via interaction of water with oxygenated functional groups that are present outside the graphitic microstructures. This interaction is characterized by a high degree of attraction, affected by pore size and site density. The dependence of the relaxation strength on the temperature of both systems shows differences, as evidenced in Fig. 5.

In the xGnP + DMF binary mixture, the relaxation strength decreased up to a solute concentration of $0.06 \text{ g}\cdot\text{mL}^{-1}$ and increased after by increasing the solute concentration, suggesting the predominance of molecular interactions [51].

In the xGnP + H₂O binary mixture, the relaxation strength increased with an increase in the temperature and decreased with an increase in the concentration over the concentration range. As the concentration of water gradually increased, various

interactions such as H-bonding, dipole-dipole and dipole induced dipole interactions occurred between molecules.

The possible presence of carboxylic, carbonyl and hydroxyl groups appears to prevent the water molecules from filling the graphene layers, whereas the removal of these groups allows water to adsorb between the layers.

The presence of oxygenated functional groups reduces the micropore volume accessible to water molecules and does not affect the micropore volume accessible to DMF molecules.

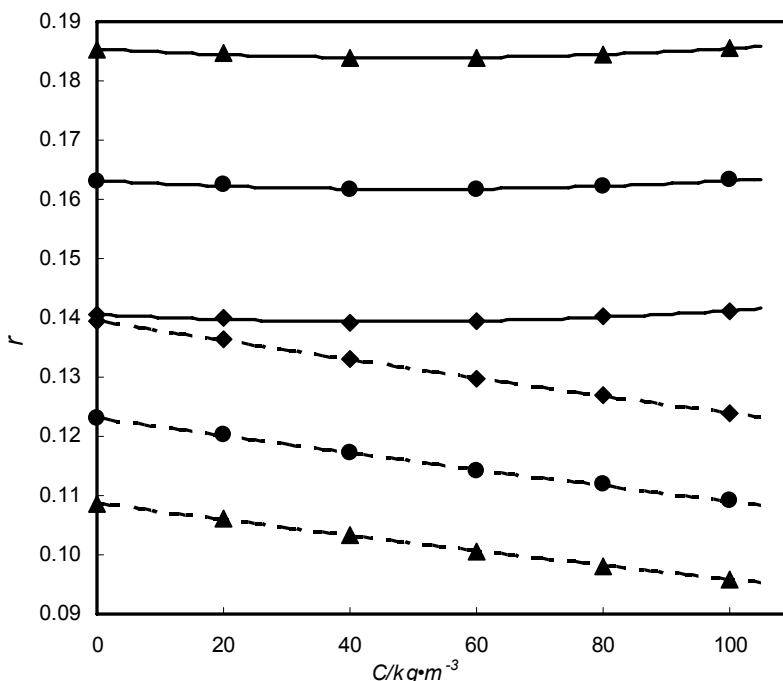


Fig. 5. Comparative representation of the relaxation strength of binary xGnP + H₂O and xGnP + DMF [19] systems versus concentration of solute at various temperatures, T/K: \blacklozenge , 293.15; \bullet , 298.15; \blacktriangle , 303.15; $-\cdot-$, for H₂O; $-$, for DMF; polynomial correlated values.

4. Conclusions

In summary we developed a novel approach of characterization for the graphene-based nanomaterials in organic and in aqueous solvents, base on the experimental determination of some thermodynamic parameters.

Considering the importance of surface chemistry in the adsorption of water, further characterization of the nature of water bonding with the functional groups is necessary. Additional thermodynamic information can be obtained by examining

the multi-temperature equilibrium data. This work renders it possible to achieve important opportunities of to use the carbon-nanostructure of graphene in composite nanomaterials for low-cost and environmental-friendly decontamination adsorbents for organic and inorganic contaminants.

Acknowledgments. The present study was carried out within the research programme Chemical Thermodynamics of *Ilie Murgulescu* Institute of Physical Chemistry, which was financed by the Romanian Academy of Sciences. Support from the EU (ERDF) and Romanian Government, which allowed for the acquisition of the research infrastructure under POS-CCE O 2.2.1 project INFRANANOCEM - Nr. 19/01.03.2009 is gratefully acknowledged.

References

- [1] A.B. BOURLINOS, V. GEORGAKILAS, R. ZBORIL, T.A. STERIOTIS, A.K. STUBOS, *Small* **5**, pp.1841–1845, 2009.
- [2] A.O. NEILL, U. KHAN, P.N. NIRMALAJ, J. BOLAND, J.N. COLEMAN, *J. Phys. Chem. C*. **115**, pp. 5422–5428, 2011.
- [3] C.E. HAMILTON, J.R. LOMEDA, Z.Z. SUN, J.M. TOUR, A.R. BARRON, *Nano Lett.* **9**, 3460–3462, 2009.
- [4] Y. HERNANDEZ, M. LOTYA, D. RICKARD, S.D. BERGIN, J.N. COLEMAN, *Langmuir* **26**, pp. 3208–3213, 2010.
- [5] J.N. COLEMAN, *Adv. Funct. Mater.* **19**, pp. 3680–3695, 2009.
- [6] C.J. SHIH, S.C. LIN, M.S. STRANO, D. BLANKSCHTEIN, *J. Am. Chem. Soc.* **132**, pp. 14638–14648, 2010.
- [7] M.S. STRANO, V.C. MOORE, M.K. MILLER, M.J. ALLEN, E.H. HAROZ, C. KITTRELL, *NanoSci. Nanotechnol.* **39**, pp. 81–86, 2003.
- [8] Y. HERNANDEZ, V. NICOLASI, M. LOTYA, F.M. BLIGHE, Z.Y. SUN, S. De, *NAT. Nanotechnol.* **3**, pp. 563–568, 2008.
- [9] C. FU, X. YANG, *Carbon* **55**, pp. 350–360, 2013.
- [10] L.D. BELYAKOVA, A.V. KISELEV, N.V. KOVALEVA, *Russ. J. Phys. Chem., Ussr.* **42**, 1204–1208, 1968.
- [11] A. STRIOLO, A.A. CHAILVO, P.T. CUMMINGS, K.E. GUBBINS, *Langmuir* **19**, pp. 8583–8591, 2003.
- [12] J.C. LIU, P.A. MONSON, *Langmuir* **21**, pp. 10219–10225, 2005.
- [13] C. RODRÍGUEZ-GONZÁLEZ, O.V. KHARISSOVA, A.L. MARTÍNEZ-HERNÁNDEZ, V.M. CASTAÑO, C. VELASCO-SANTOS, *Dig. J. Nanomater. Bios.* **8**, pp. 127–138, 2013.
- [14] V.T. NGUYEN, D.D. Do, D. NICHOLSON, *Carbon* **66**, pp. 629–636, 2014.
- [15] X. LI, L. LI, Y. WANG, H. LI, X. BIAN, *J. Phys. Chem. C* **117**, pp. 14106–14112, 2013.
- [16] A.C. ION, A. ALPATOVA, I. ION, A. CULETU, *Materials Science and Engineering B* **176**, pp. 588–585, 2011.
- [17] A.C. ION, I. ION, A. CULETU, *Materials Science and Engineering B* **176**, pp. 504–509, 2011.
- [18] F. ROUQUEROL, J. ROUQUEROL, K.S.W. SING, *Adsorption by powders and Porous Solids*, Academic Press, London, 1999.
- [19] J.Y. BRENNAN, T.J. BANDOSZ, K.T. THOMPSON, K.E. GUBBINS, *Colloids Surf.* **A539**, pp. 187–188, 2001.
- [20] L. ZHOU, Y. SUN, Y.P. ZHOU, *AIChEJ* **48**, pp. 2412–2416, 2002.

- [21] M. TAGAWA, M. IKEMURA, Y. NAKAYAMA, Y. OHMAE, *Tribol. Lett.* **17**, pp. 575–580, 2004.
- [22] C.M. WHITE, D.H.SMITH, K.L. JONES, A.L. GOODMAN, S.A. JIKICH, R.B. LAKOUNT, S.B. DU BOSE, E. OZDEMIR, B.I. MORSI, K.T. SCHROEDER, *Energy Fuels* **19**, pp. 659–724, 2005.
- [23] O. IULIAN, F. SIRBU, C. STOICESCU, *Rev. Roum. Chim.* **53**, pp. 1125–1129, 2008.
- [24] F. SIRBU, O. IULIAN, *J. Chem. Eng. Data* **55**, pp. 3853–3858, 2010.
- [25] F. SIRBU, O. IULIAN, A.C. ION, I. ION, *J. Chem. Eng. Data* **56**, pp. 4935–4943, 2011.
- [26] I. ION, F. SIRBU, A.C. ION, *J. Chem. Eng. Data* **58**, pp. 1212–1222, 2013.
- [27] M.M. PALAIOLOGOU, G.K. ARIANAS, N.G. TSIERKEZOS, *J. Solution Chem.* **35**, pp. 1551–1565, 2006.
- [28] W. WAGNER, A. PRUSS, *J. Phys. Chem. Ref. Data* **31**, pp. 387–535, 2002.
- [29] A.F.S.S. MENDONÇA, F.A. DIAS, I.M.S. LAMPREIA, *J. Solution Chem.* **36**, pp. 13–26, 2007.
- [30] A.V. RAYER, K.Z. SUMON, A. HENNI, P. TONTIWACHWUTHIKUL, *J. Chem. Thermodyn.* **43**, pp. 1897–1905, 2011.
- [31] I.B. MALHAM, M. TURMINE, *J. Chem. Thermodyn.* **40**, pp. 718–723, 2008.
- [32] D.R. LIDE, *CSIR Handbook of Chemistry and Physics*, 7th ed., 1990–1991.
- [33] A. ARCE, A. BLANCO, A. SOTO, I. VIDAL, *J. Chem. Eng. Data* **38**, pp. 336–340, 1993.
- [34] J.A. RIDDICK, W.B. BUNGER, T.K. SAKANO, *Organic Solvents: Physical Properties and Methods of Purification*. 4th edn. Wiley, New York, 1988.
- [35] M.N. ROY, R. CHANDA, G. GHOSH, *Russ. J. Phys. Chem.* **A83**, pp. 1331–1341, 2009.
- [36] B.R. SHINDE, S.S. JADHAV, S.U. SHINDE, D R. SHENGULE, K.M. JADHAV, *Arch. Phy. Res.* **2**, pp. 107–113, 2011.
- [37] A. TOUMI, M. BOUANZ, *J. Mol. Liq.* **139**, pp. 55–60, 2008.
- [38] I.M.S. LAMPREIA, Â.F.S. SANTOS, *J. Sol. Chem.* **39**, pp. 808–819, 2010.
- [39] U.S. VURAL, V. MURADOGLU, S. VURAL, *Bull. Chem. Soc. Ethiop.* **25**, pp. 111–118, 2011.
- [40] Evaluation of measurement data-guide to the expression of uncertainty in measurement. Report of Working Group 1 of the Joint Committee for Guides in Metrology, 2008.
- [41] C. GONZALEZ, J.M. RESA, J. LANZ, M. IGLESIAS, *J. Food Eng.* **77**, pp. 152–161, 2006.
- [42] J.S. ROWLINSON, F.L. SWINTON, *Liquid and Liquid Mixtures*, Butterworths, London, 3rd ed., 1982.
- [43] N.G. GERECZE, *Acoustica* **38**, pp. 51–57, 1977.
- [44] G.A.C.M. SPIERINGS, G.P. MELIS, *J. Mater. Sci.* **16**, pp. 1059–1062, 1981.
- [45] V.N. REDDY, K.S.W.K. RAO, M.C.S. SUBHA, K.C. RAO, presented at International Conference on Advances in Polymer Technology 356, 26-27 Feb., India, 2010.
- [46] R.D. ALLEN, *Am. Mineralogist* **41**, pp. 245–257, 1956.
- [47] Y. LIANG, D. WU, X. FENG, K. MULLER, *Adv. Mater.* **21**, pp. 1679–1683, 2009.
- [48] D. CHEN, H. FENG, J. Li, *Chem. Rev.* **112**, pp. 6027–6053, 2012.
- [49] K. YANG, B. XING, *Chem. Rev.* **110**, pp. 5989–6008, 2010.
- [50] S.W. RUTHERFORD, *Langmuir* **22**, pp. 9967–9975, 2006.
- [51] D.R. DREYER, S. PARK, C.W. BIELAWSKI, R.S. RUOFF, *Chem. Soc. Rev.* **39**, pp. 228–240, 2010.